Check for updates

ZHU Honglin (Orcid ID: 0000-0001-8724-2835)
Schett Georg (Orcid ID: 0000-0001-8740-9615)
Hoffmann Markus (Orcid ID: 0000-0001-9698-9922)

Reset of inflammatory priming of joint tissue and reduction of the severity of arthritis flares by bromodomain inhibition

#Jasna Friščić[1,2,3], PhD; #Christiane Reinwald[1,2], PhD; Martin Böttcher[4,5,6], PhD; Miranda Houtman[7], PhD; Maximilien Euler[1,2], MS; Xi Chen[1,2], MS; Kellie I Walker[7], Philipp Kirchner[8], PhD; Honglin Zhu[9], MD; Benjamin Wirth[1,2], MD; Daniela Weidner[1,2], René Krüger[8,10], MS; Vladimir Trajkovic[11], MD; Arif B Ekici[8], PhD; Kerstin Klein[12,13], PhD; Dimitrios Mougiakakos[4,5,6], MD; Caroline Ospelt[7], MD; Georg Schett[1,2], MD; Markus H Hoffmann[1,2,3]*, PhD

[1] Department of Internal Medicine 3 - Rheumatology and Immunology, Friedrich-Alexander University Erlangen-Nürnberg (FAU) and Universitätsklinikum Erlangen, Erlangen, Germany.
[2] Deutsches Zentrum fuer Immuntherapie, Friedrich-Alexander Universität Erlangen-Nürnberg (FAU) and Universitätsklinikum Erlangen, 91054 Erlangen, Germany.
[3] Department of Dermatology, Allergy, and Venereology, University of Lübeck, Lübeck, Germany
[4] Department of Medicine 5 for Hematology and Oncology, Friedrich-Alexander-Universität Erlangen-Nürnberg, 91054 Erlangen, Germany.
[5] Department of Hematology and Oncology, University Hospital Magdeburg, Otto-von-Guericke University Magdeburg, 39120 Magdeburg, Germany
[6] sHealth Campus Immunology, Infectiology and Inflammation (GCI3), Medical Center, Otto-von-Guericke University Magdeburg, 39120 Magdeburg, Germany
[7] Center of Experimental Rheumatology, Department of Rheumatology, University Hospital Zurich, University of Zurich, Zurich, Switzerland.
[8] Institute of Human Genetics, Friedrich-Alexander Universität Erlangen-Nürnberg (FAU) and Universitätsklinikum Erlangen, 91054 Erlangen, Germany
[9] Department of Rheumatology, Xiangya Hospital, Central South University, Changsha, Hunan, 410008, P.R China.
[10] Department of Nephrology and Hypertension, Friedrich-Alexander-Universität Erlangen-Nürnberg (FAU) and Universitätsklinikum Erlangen, 91054 Erlangen, Germany
[11] Institute of Microbiology and Immunology, Faculty of Medicine, University of Belgrade, 11000 Belgrade, Serbia
[12] Department of BioMedical Research, University of Bern, Bern, Switzerland
[13] Department of Rheumatology and Immunology, University Hospital Bern, Bern, Switzerland

#These two authors contributed equally to this work

*Lead contact:

Dr. Dr. Markus Hoffmann, Ratzeburger Allee 160, 23562 Lübeck, phone: +49-451-31019120, email: markus.hoffmann@uni-luebeck.de

This article has been accepted for publication and undergone full peer review but has not been through the copyediting, typesetting, pagination and proofreading process which may lead to differences between this version and the Version of Record. Please cite this article as doi: 10.1002/art.42378

This article is protected by copyright. All rights reserved.

Accepted Article

source: https://doi.org/10.1002/art.42378 | downloaded: 4.5.2024

23265205, ja, Downloaded from https://onlinelibrary.wiley.com/doi/10.1002/art.42378 by Universität Bern, Wiley Online Library on [18/10/2022]. See the Terms and Conditions (https://onlinelibrary.wiley.com/terms-and-conditions) on Wiley Online Library for rules of use; OA articles are governed by the applicable Creative Commons License

Key words:
inflammation, arthritis, inflammatory tissue priming, synovial fibroblasts, epigenetics, bromodomain and extra-terminal motif proteins

Abstract

Objective: We have recently shown that priming of synovial fibroblasts (SFs) drives arthritis flares. Pathogenic priming of SFs is essentially mediated by epigenetic reprogramming. Bromodomain and extra-terminal motif (BET) proteins translate epigenetic changes into transcription. Here we used a BET inhibitor to target inflammatory tissue priming and reduce flare severity in experimental arthritis.

Methods: BALB/c mice were treated intraperitoneally or locally into the paw with I-BET151, which blocks interaction of BET proteins with acetylated histones. Effect of I-BET151 on acute arthritis and/or inflammatory tissue priming was assessed in a model of repeated injections of monosodium urate crystals or zymosan into the paw. I-BET151 was given either from before arthritis induction, at peak inflammation, or after healing of the first arthritis bout. Transcriptomic (RNA-Seq), epigenomic (ATAC-Seq) and functional analysis (invasion, cytokine production, migration, senescence, metabolic flux) was performed on murine and human SFs treated with I-BET151 *in vitro* or *in vivo*.

Results: Systemic I-BET151 administration did not affect acute inflammation but abolished inflammatory tissue priming and diminished flare severity in both preventive and therapeutic treatment settings. I-BET151 was also effective when applied locally in the joint. BET inhibition also inhibited osteoclast differentiation, while macrophage activation in the joint was not affected. Flare reduction after BET inhibition was mediated, at least in part, by rolling back the primed transcriptional, metabolic and pathogenic phenotype of SFs.

Conclusion: Inflammatory tissue priming is dependent on transcriptional regulation by BET proteins, which makes them promising therapeutic targets for preventing arthritis flares in previously affected joints.

Accepted Article

23265205, ja, Downloaded from https://onlinelibrary.wiley.com/doi/10.1002/art.42378 by Universität Bern, Wiley Online Library on [18/10/2022]. See the Terms and Conditions (https://onlinelibrary.wiley.com/terms-and-conditions) on Wiley Online Library for rules of use; OA articles are governed by the applicable Creative Commons License

Accepted Article

23265205, ja, Downloaded from https://onlinelibrary.wiley.com/doi/10.1002/art.42378 by Universität Bern, Wiley Online Library on [18/10/2022]. See the Terms and Conditions (https://onlinelibrary.wiley.com/terms-and-conditions) on Wiley Online Library for rules of use; OA articles are governed by the applicable Creative Commons License

Introduction

Virtually all forms of arthritis are characterized by transient increases in local inflammatory disease activity, heralded by pain, joint swelling and other concomitant symptoms. These episodes, often termed "flares" vary widely in frequency, duration and intensity, but tend to become progressively more severe and frequent in those not receiving adequate therapy. Flares also strongly increase in their frequency once anti-inflammatory treatment is tapered or withdrawn (1). While flares seriously impair life quality of individuals with arthritis, little is known about their underlying mechanisms. As flares often recur at sites that have been previously affected by arthritis (2) it has been considered that a sensitization of local tissue occurs in the context of inflammation that renders affected sites more prone for flares.

In arthritis, inflammation is orchestrated by resident synovial cells. Certain macrophage and fibroblast subsets that are predominantly found in the synovial sublining are associated with inflammation and flares in human and murine arthritis (3-5). We have recently shown that a complement C3 expressing synovial fibroblast (SF) subset is instrumentally involved in sensitizing synovial tissue for inflammation ("inflammatory tissue priming") (6). Transfer of these SFs to healthy joints is sufficient to induce a primed state in the tissue that exacerbated subsequent flares of arthritis, demonstrating that these cells are central drivers of inflammatory tissue priming.

Primed SFs are getting functionally and epigenetically reprogrammed by repeated inflammatory insults (6). Tackling the epigenetic alterations associated with SF priming might therefore be an important means to modulate arthritis flares. Small molecule inhibitors targeting bromodomain and extra-terminal motif (BET) proteins are an attractive class of compounds able to target epigenetic changes in the context of inflammation (7). BET proteins are very conserved from yeast to humans and crucial for embryogenic development (8), highlighting their prominent role for gene regulation. BET proteins contain tandem arrangements of bromodomains (BRD) that 'read' chromatin states by binding to acetylated histones and actively regulate gene expression by acting as a scaffold that enables the recruitment and binding of protein complexes or function as methyltransferases, ATP-depending chromatin remodeling complexes, histone acetyl transferases (HATs), helicases, and transcription factors themselves (9, 10). For example, BRD4, the best studied BET protein, plays an active role in transcription, e.g. via regulating the transcriptional activity of NF-κB (11). BET proteins, unlike other acetylated histone-binding proteins, remain associated with acetylated histones during cell division (12) and are therefore thought to contribute to the transmission of transcriptional memory to the next cell generation. BET inhibitors bind to BRDs, compete for binding to acetylated histones and are also able to displace already bound BET proteins from chromatin, thus potentially being able to prevent or even revert inflammatory tissue priming.

In the current study, we show that I-BET151, a histone mimetic targeting the BET proteins BRD2, BRD3, BRD4, and BRDT (13), inhibited worsening of iterated arthritis in mice while not affecting acute inflammation. I-BET151 was efficacious in both preventive and therapeutic treatment settings, thus abrogating and rolling back inflammatory tissue priming. Mechanistically, I-BET151 rectified the primed transcriptional, metabolic and functional inflammatory state of mouse-derived and human SFs. Osteoclast differentiation was also affected by I-BET151, which might contribute to the amelioration of pathologic bone remodeling associated with inflammatory tissue priming. Although

previous studies have shown anti-inflammatory and bone protective action of BET inhibitors in experimental arthritis (7), *in vivo* effects on SFs, and a role of BET proteins in inflammatory tissue priming had not been studied yet. Our data provide evidence that I-BET151 is an attractive candidate to mitigate flare severity in chronic inflammatory diseases of the joints.

Materials and Methods

Animals

BALB/c mice were bred and kept at the University of Erlangen, Germany, or the Faculty of Medicine, University of Belgrade, Serbia with free access to food and water and 12h light/dark cycles. The animal studies were approved by the local ethical committees in Erlangen and Belgrade and conducted according to the guidelines of the Federation of European Laboratory Animal Science Associations. Experiments were performed in healthy 8-12 weeks old mice, both male and female, using age- and sex-matched littermate controls. Mice were allocated randomly into groups by a computer-based random number generator (http://www.randomizer.org), so that each cage contained animals of every group to compensate for possible cage effects.

Inflammatory arthritis model in mice

Monoarthritis was induced by injection of 1.4 mg monosodium urate (MSU) crystals or 300 µg zymosan suspended in 70 µl sterile PBS into the foot pads of the hind paws, between the metatarsals. MSU crystals were generated in house in a lipopolysaccharide-free manner as described (14), zymosan was purchased from Sigma-Aldrich. On day 0, MSU crystals or zymosan were injected only into the left paw while the right paw remained untreated. After resolution of the first arthritis episode (defined as reduction of paw thickness to <110% of values before injection, usually occurring between day 9 and 14), MSU crystals or zymosan were then injected into both paws. Paw thickness was monitored with an electronic caliper (Kroeplin). Priming indices were defined as the ratio between the AUC of the second arthritis episode and the AUC of the simultaneously occurring first arthritis episode in the contralateral paw.

Analysis of features of murine arthritis

For immunohistochemistry and histomorphometry, paws taken from naïve mice or 9 days after the second injection of MSU crystals or zymosan were fixed overnight in 4% formalin, decalcified with 14% EDTA (pH 7.2 in NH_4OH), and embedded in paraffin. Paraffin sections were stained with tartrate-resistant acid phosphatase for assessment of bone erosions and enumeration of osteoclasts. Analyses were performed on a Nikon microscope equipped with a digital quantification system (OsteoMeasure). For staining pathogenic fibroblasts, sections were incubated with a rabbit anti-mouse Cadherin 11 antibody (Invitrogen PA5-96937, 1:200) and horseradish peroxidase (HRP)-conjugated goat-anti-rabbit secondary antibody (Southern Biotech, cat. #4030-05, 1:400 in blocking buffer). The HRP substrate 3,3'-diaminobenzidine (Vector Labs DAB-kit #SK4100) was used as substrate for HRP.

Microcomputed tomography (µCT) of the metatarsal and tarsal areas of mice was performed using the cone-beam Desktop Micro Computer Tomograph "µCT 40" by SCANCO Medical AG, Bruettisellen, Switzerland. The scan settings were optimized for calcified tissue visualization at 55 kVp, 145 µA, with 200 ms integration time and a voxel size of 8,0 µm was chosen. For the 3D-segmentation of bone-volumes the "µCT Evaluation Program Version 6.6" by SCANCO was used to convert the acquired tomographic data into TIFF format, followed by surface rendering using the Image Analysis Software

Accepted Article

23265205, ja, Downloaded from https://onlinelibrary.wiley.com/doi/10.1002/art.42378 by Universität Bern, Wiley Online Library on [18/10/2022]. See the Terms and Conditions (https://onlinelibrary.wiley.com/terms-and-conditions) on Wiley Online Library for rules of use; OA articles are governed by the applicable Creative Commons License

IMARIS Version 9.7.0 (Oxford Instruments). Using SCANCO´s operating system "Open VMS" osteophyte volumes were manually defined as volume of interest along the bones. Then greyscale thresholds were set to include all voxels related to bone tissue for the measurement of bone volume.

Treatment of murine arthritis with the pan BET inhibitor I-BET151

For inhibition of BET proteins, mice were treated with 20 mg/kg I-BET151 (GlaxoSmithKline, GSK1210151A) by daily i.p. injections. Control mice received daily i.p. injections of vehicle (10% w/v Kleptose, Hydroxypropyl β-cyclodextrin in 0.9%/g saline). We followed 3 systemic treatment protocols (see Fig. 1A): Group 1 and 1b: Preventive treatment with I-BET 151 or vehicle, starting 1 or 5 days before the first injection, respectively, and continued until the end of the experiment. Group 2: Therapeutic treatment with I-BET151 or vehicle, starting 2-3 days after the disease peak and continued for 6 days. Group 3: Resetting of epigenetic programming after the first arthritis episode had healed (4 days treatment). For local treatment, mice received 6 daily subcutaneous injections of 20 mg/kg I-BET151 or vehicle in the paw after remission of the initial bout of MSU crystal-induced arthritis. The DNA-methyltransferase inhibitor 5-aza-2´-deoxycytidine (decitabine, Sigma-Aldrich) was applied i.p. 0,4 mg/kg twice weekly, and the histone deacetylase inhibitor Trichostatin A (Sigma-Aldrich) at 5 mg/kg every other day.

Isolation and culturing of synovial fibroblasts (SFs) from mouse paws

SFs were isolated from the paws of mice after one/two MSU- or zymosan-injections, and from non-injected naïve paws. SF cell suspensions of murine paws were prepared by gently rocking dissected and skin-flayed paws for 1 hour at 37°C in DMEM containing 1 mg/ml collagenase type IV (Worthington Biochemicals, #LS004188). Cells derived from 2 to 3 paws were pooled and cells were then grown in DMEM (Gibco) supplemented with 10% heat-inactivated calf serum, (glucose (4.5 g/L), L-glutamine 2 mM), penicillin and streptomycin (1% each) antibiotics, and 1% fungizone (Amphotericin B, Sigma Aldrich). Medium was changed twice a week. SFs between passages 4 and 8 were used for the experiments and contained less than 2% $CD45^+$ or $CD31^+$ cells, as determined by flow cytometry with a PerCP Cy5.5 conjugated anti-CD45 antibody (Biolegend, #103132) and an AF647-conjugated anti-CD31 antibody (Biolegend, #102516). Alternatively, we used flow cytometry sorted $CD45^-CD31^-$ SFs.

Cell sorting of murine synovial fibroblasts by flow cytometry

Cultured SFs were detached at passage 2 from flasks by CorningTM Cell stripper (#15313661; Fisher scientific) and stained in FACS buffer (PBS, 10% FCS, 0.5 mM EDTA) with a PerCP Cy5.5 or an APC-conjugated anti-CD45 antibody (Biolegend. #103132 and #103112), a BV421-conjugated anti-CD31 antibody (Biolegend, #102423) and Sytox Green (Thermofisher S7020). After washing, Sytox $Green^+$ (dead) cells, $CD45^+$ and $CD31^+$ cells were sorted out on a FACS Aria machine. $CD45^-CD31^-$ remaining SF were used after re-culturing.

Flow cytometric analysis of digested mouse paws

Paws were digested as described above, cell isolates were stained witn Ghost Dye™ Red 710 (Tonbo, San Diego, USA) according to the manufacturer´s recommendation and fixed with BD Cytofix™ Fixation buffer. Samples were stained after blocking of the FcR using mouse FcR blocking reagent (Miltenyi Biotec, Bergisch-Gladbach, Germany) with the following antibodies: CD45-PerCP/Cy5.5 (clone 30-F11, Biolegend), CD31-BV510 (clone 390, BD Bioscience), CD90.2-FITC (clone 53-2.1, Biolegend), Podoplanin-PE (clone eBio 8.1.1, Thermo Fisher Scientific), CD11b-BV750 (clone M1/79, Biolegend), Ly6C-PacificBlue (clone HK1.4, Biolegend), F4/80-Pe/Cy7 (clone BM8, Biolegend), and I-A/I-E-APC/Cy7 (clone M5/114.15.2, Biolegend). Stained samples were recorded after proper spectral

Accepted Article

23265205, ja, Downloaded from https://onlinelibrary.wiley.com/doi/10.1002/art.42378 by Universität Bern, Wiley Online Library on [18/10/2022]. See the Terms and Conditions (https://onlinelibrary.wiley.com/terms-and-conditions) on Wiley Online Library for rules of use; OA articles are governed by the applicable Creative Commons License

unmixing on a Cytek NL-3000 and data were analysed using SpectroFloR V3 (Scytek Biosciences, Freemont, USA) and FlowJo V10 (BD Biosciences).

Human synovial fibroblasts

Rheumatoid arthritis (RA)-derived SFs were obtained from synovial tissue specimens from patients fulfilling the RA classification criteria (15) during joint replacement surgery at the Department of Orthopedic Surgery, Schulthess Clinic Zurich, Switzerland. All participants gave written informed consent as approved by the local ethic committees. For patient characteristics see Table S1.

SFs from healthy human synovium were purchased from Innoprot (#P10972) and primed *in vitro* by repeated incubation with TNFα. To this end we followed a previously published protocol (16): 24h after seeding, SFs were stimulated with 10 ng/ml recombinant human TNF (Immunotools) for 24h. Afterwards, cells were washed twice with PBS, left untreated for 24h, followed by a second stimulation with TNF (10 ng/ml) for another 24h.

All human SFs were cultured as described (17) and used between passages 4 to 8 for experiments.

Complement C3 activation analysis in human RA-SF by Western blot

RA-SF were repeatedly stimulated with TNFα and simultaneously treated with I-BET151 (1 µM) or vehicle (DMSO, 1:10.000). Cells were then lysed in Laemmli buffer (BioRad) for Western blotting after a total treatment period of 72h. Lysates were separated on 10% SDS polyacrylamide gels and electro-blotted onto nitrocellulose membranes (Whatman). Membranes were blocked for 1h in 5 % (w/v) non-fat milk in TBS-T (20 mM Tris base, 137 mM sodium chloride, 0.1 % Tween 20, pH 7.6) and probed with antibodies against the C3 α-chain (EPR2988; Abcam), or α-tubulin (ab11304; Abcam). As secondary antibodies, horseradish peroxidase-conjugated goat anti-rabbit or goat anti-mouse antibodies (#2307391 and #10015289 Jackson ImmunoResearch) were used. Signals were detected using an ECL Western blotting detection reagent (GE Healthcare) and the Alpha Imager Software-system (Alpha Innotech). Expression analysis of specific proteins was performed by pixel quantification of the electronic image.

RNA Sequencing and qPCR (transcriptomic analysis)

Isolation of RNA from mouse or human SFs was performed using the RNeasy kit from Qiagen (#74104). One microgram of total RNA was reverse transcribed and real-time quantitative PCR was performed on a Bio-Rad CFX96 Touch Real-Time PCR Detection System using qPCR Master Mix Plus for SYBR Green (Eurogentec RT-SN2X-03). Normalized gene expression values were calculated as the ratio of expression of mRNA of interest to the expression of reference gene (*β-actin* or *RPLP0*). Primer sequences were as follows:

Gene	Forward (5´- 3´)	Reverse (5´- 3´)	Reference
Actb	TGTCCACCTTCCAGCAGATGT	AGCTCAGTAACAGTCCGCCTAGA	(18)
P15 (*Cdkn2b*)	AGATCCCAACGCCCTGAAC	CCCATCATCATGACCTGGATT	(19)
$P16^{INK4}$ (*Cdkn2a*)	CCCAACGCCCCGAACT	GCAGAAGAGCTGCTACGTGAA	(20)
P21 (*Cdkn1a*)	GCAGATCCACAGCGATATCCA	AACAGGTCGGACATCACCAG	(20)

For bulk RNA Sequencing of cultured murine or human SFs sequencing libraries were prepared using the TruSeq stranded mRNA kit (Illumina, 20020594) from 1 µg RNA. Libraries were subjected to single-end sequencing (101 bp) on a HiSeq-2500 platform (Illumina). The obtained reads were demultiplexed and converted to FASTQ format using bcl2fastq v2.17.1.14. Quality filtering was performed using cutadapt v. 1.18; total RNA libraries were alternatively filtered against a library of rRNA, tRNA, mt-rRNA and mt-tRNA sequences. Filtered reads were mapped to the mouse or human reference genome (Ensembl GRCm38) using the splice-aware aligner STAR (total RNA: STAR v 2.4.0i; mRNA: STAR v 2.6.1c). Read counts per gene were obtained by summing up reads for non-

Accepted Article

23265205, ja, Downloaded from https://onlinelibrary.wiley.com/doi/10.1002/art.42378 by Universität Bern, Wiley Online Library on [18/10/2022]. See the Terms and Conditions (https://onlinelibrary.wiley.com/terms-and-conditions) on Wiley Online Library for rules of use; OA articles are governed by the applicable Creative Commons License

overlapping exons using Ensembl gene models (total RNA: HTSeq count, Ensembl annotation v84; mRNA: Subread v1.6.1, Ensembl annotation v96). The subsequent analyses were performed using the R package DESeq2 (21) (R v3.6.1, DESeq2 v1.24.0).

Abundances of sublining (SL) and lining layer (LL) cell clusters were enumerated from bulk RNA sequencing data by CIBERSORTx (22), using previously published single-cell reference profiles (6) to generate a gene signature matrix for each cluster. Then, the absolute SL and LL fibroblast fraction scores were calculated with S-mode batch correction, disabled quantile normalization, run mode absolute and 1000 permutations.

ATAC Seq

ATAC-seq library preparation was performed on cultured, FACS sorted $CD45^{-}CD31^{-}$ MSU/MSU SFs (35,000 cells per sample) after 12h treatment with 1 µM I-BET151 or vehicle (DMSO, 1:10,000*) in vitro* using the ATAC-seq kit from Active motif (#13150). In short, nuclei were isolated by adding 100µl ice cold ATAC-lysis buffer to the cell pellet and resuspending cells with a pipette. After centrifugation (500 g, 10 min at 4°C), cells were washed and incubated with the tagmentation master mix in a shaking heat block at 37°C/800 rpm for 30 minutes. Obtained DNA was taken up in DNA purification buffer, purified using the contained DNA purification columns, amplified for 10 cycles using indexed primers, and size-selected using SPRI bead solution. A quality control (QC) was performed in order to verify the size distribution of the PCR enriched library fragments. To this end, aliquots of the DNA libraries were analyzed on an Agilent Technologies 2100-Bioanalyzer, using a High Sensitivity DNA chip. This Bioanalyzer based QC was for qualitative purposes only. A precisely quantification of the libraries was done using the Qubit dsDNA HS Assay Kit (Thermo Fisher Scientific).

The bar-coded amplicons from ATAC-Library preparation were sequenced on a HiSeq 2500 platform (Illumina). Single-end reads were quality filtered according to the standard Illumina pipeline, de-multiplexed and fastq files were generated. The data were analyzed using the nf-core/atacseq pipeline (v1.2.1) (10.5281/zenodo.2634132) with standard settings. Reads were aligned to GRCm38 and MACS2 broad peaks were called. Peaks found in at least two biological replicates were kept for further analysis. Peaks were annotated relative to gene features using HOMER. Differential accessibility regions were determined using DESeq2 (v1.28.1).

Functional and metabolic testing of synovial fibroblasts

Analysis of the barrier function properties and migratory capacity of SFs. A Matrix-associated transepithelial resistance invasion (MATRIN-) assay was utilized as described (6) for testing the SFs' invasive potential into extracellular matrix. In short, disturbing the integrity of an MDCK-C7 epithelial cell monolayer by invading SFs leads to a decrease of the transepithelial electrical resistance measured with a set of electrodes connected to an ohmmeter. The electrical resistance was measured twice a day. All measurements were performed in triplicates and were terminated after total breakdown of electrical resistance.

We also used a transwell matrix-invasion assay for analyzing the invasive capacity of murine Trichostatin A (TSA)- and human I-BET151 treated SFs, using Matrigel coated Corning Invasion Chamber with 8 µm pore size, as described (23). To this end, control SFs or SFs treated with TSA (1 µM, 24h) or I-BET151 (1 µM, 24h) were resuspended in 0.5% bovine serum albumin (BSA)/DMEM and seeded at 15,000 cells per well in the upper chamber. Recombinant murine PDGFBB (E33856, Peprotech) solution (50 ng/ml) in 0.5% BSA/DMEM was used to promote invasion of SFs. Non-invading cells together with Matrigel were removed after 48h, and the cells on the lower surface of

Accepted Article

23265205, ja, Downloaded from https://onlinelibrary.wiley.com/doi/10.1002/art.42378 by Universität Bern, Wiley Online Library on [18/10/2022]. See the Terms and Conditions (https://onlinelibrary.wiley.com/terms-and-conditions) on Wiley Online Library for rules of use; OA articles are governed by the applicable Creative Commons License

the membrane were stained with 0.4% crystal violet (C0775, Sigma Aldrich) and counted with a Nikon microscope.

Wound healing and migration assay. For analysis of SF migration/proliferation we used a wound-healing assay with culture inserts (ibidi, #80209) in 6-well culture dishes. 20,000 SFs were placed in 70 µl culture medium per chamber of an insert. After 24h, the inserts were removed and the well was filled with 2 ml culture medium. The change in SF-covered area over time was monitored on a microscope equipped with a temperature and CO_2 control chamber (Keyence) and quantified using Photoshop CS6 (Adobe).

3D organoids. The formation of an organized synovial lining was analysed in 3D synovial organ cultures (micromasses) as previously described (24). SFs were harvested from the cultures and resuspended in Matrigel Matrix (BD Biosciences) at a density of $1x10^6$ cells/ml. The obtained Matrigel Matrix cell suspension was plated in cell culture plates coated with 1% Poly-2-hydroxyethylmethaacrylate (poly-HEMA, Sigma-Aldrich). After 35-50 min incubation at 37°C, 2ml Micromass-Medium was added. SFs were maintained in culture in DMEM/F12 (Gibco) supplemented with 10% FCS, 0.1 mM ascorbic acid, ITS supplement (BioWhittaker) and 1% penicillin-streptomycin at 5% CO_2, 37°C for 3 weeks until the organ culture had built a sphere. During these 3 weeks, medium was changed twice per week. For analysis of 3D organ cultures, paraffin-embedded sections were stained with an antibody to vimentin and DAPI. Lining layer thickness and interconnectivity in the sublining were determined on section images using Photoshop CS6 (Adobe).

Concentrations of cytokines and chemokines in supernatants of 3D organoids were measured after 3 weeks culture by a flow cytometry-based bead assay (BioLegend).

Extracellular flux analysis. Bioenergetics were analyzed using a Seahorse XFe96 (Agilent, Santa Clara, CA) as previously described (6). Briefly, 3 x 10^4 SFs were seeded per well in heptaplicates into Seahorse XF culture plates and incubated overnight at 37°C, 5%CO_2. Next day, medium was replaced by glucose-free (glycolysis stress test, GST) or glucose-containing DMEM (mitochondrial stress test, MST) with tightly adjusted pH and samples were incubated an additional 1h in a CO_2-free atmosphere. Samples' extracellular acidification rate (ECAR, as surrogate for aerobic glycolysis) and oxygen consumption rate (OCR, as surrogate for mitochondrial respiration) were recorded after sequential injection of glucose, oligomycin, and 2-DG for the GST or oligomycin, FCCP, and antimycin A/rotenone for the MST. Last, total protein content per well was determined using the Pierce™ BCA Protein Assay Kit (Thermo Fisher Scientific, Waltham, MA) to normalize the recorded raw data. Resulting data was converted to csv-files using the Wave Desktop Software and metabolic parameters were calculated with Microsoft Excel. GraphPad Prism 9 was used for visualization and statistical analysis.

Analysis of senescence. For detection of senescence associated β-galactosidase (SA-β-Gal), SFs from healthy mice or healthy human synovium were stimulated with 10 ng/ml TNFα on flat bottom 12-well plates for 24h. After washing with PBS, cells were left untreated for 24h in standard fibroblast medium, followed by a second stimulation with TNFα (10 ng/ml) for another 24h. Control cells were incubated without any stimulation with TNFα. Treatment with 1 µM I-BET151 or vehicle was conducted simultaneously with TNf stimulation. SA-β-Gal activity was then visualized with a senescence detection kit (Abcam, 65351). The number of SA-β-Gal$^+$ SFs was determined counting positively stained and total number of cells in three visible fields per sample.

Induction of inflammatory tissue priming by injection of fibroblasts into the paw

Left paws of mice were injected with MSU crystals at day 0. After the resolution of the inflammation, at day 15, 500 x 10^3 flow cytometry-sorted SFs from naïve (-/-) or primed (MSU/MSU) paws that had been pretreated *in vitro* with 1 µM I-BET151 or vehicle for 12h were transferred to contralateral

Accepted Article

23265205, ja, Downloaded from https://onlinelibrary.wiley.com/doi/10.1002/art.42378 by Universität Bern, Wiley Online Library on [18/10/2022]. See the Terms and Conditions (https://onlinelibrary.wiley.com/terms-and-conditions) on Wiley Online Library for rules of use; OA articles are governed by the applicable Creative Commons License

paws by subcutaneous injection between the metatarsals. After three days, arthritis was initiated in both paws by the injection of MSU crystals. A scheme of the SF transfer model is shown in Fig. 4A.

Osteoclast differentiation

Bone marrow cells were isolated from tibia and femur of 8-week-old Balb/c mice using DMEM. Red blood cells were lysed using cold lysis buffer (155 nM NH_4Cl, 10 mM $KHCO_3$, 0.1 mM EDTA, pH 7). Cells were plated in a 6-well cell culture plate and incubated at 37°C/5% CO_2 overnight. The following day, non-adherent cells (200 x 10^3 well) were added to 96-well plates in αMEM supplemented with 10% FCS, 1% Penicillin-Streptomycin, 30 ng/ml recombinant murine M-CSF (PeproTech, #315-02) and 10 ng/ml recombinant murine RANKL (PeproTech 315-11). From the second day after plating, pre-osteoclasts were treated with 0.01 µM, 0.1 µM or 1 µM IBET-151 or vehicle (DMSO, 1:10.000). After 5 days, cells were fixed and stained for TRAP activity using a commercially available kit (Sigma, 387A-1KT). TRAP-positive multinucleated cells, designated as osteoclasts, were counted by light microscopy and numbers of nuclei were determined.

Statistical analysis

Two group comparisons were performed using unpaired or paired 2-tailed Student's t-test or, in the case of non-normally distributed data, by 2-tailed Mann-Whitney U test. Gaussian distribution of samples was checked using Kolmogorov-Smirnov normality test. Within each set of experiments shown in one graph multiple comparisons of groups were adjusted using Tukey's (if the mean of each group was compared to the mean of every other group) or Sidak´s (if the means of selected pairs of groups were compared) multiple comparisons test, or Dunnett's test if several values were compared to a control value. Computations and charts were performed using GraphPad Prism 9.0 software. Unless indicated otherwise, figures show means ± S.E.M. Levels of significance are indicated as follows throughout the manuscript: *$p < 0.05$, **$p < 0.01$, ***$p < 0.001$.

Results

BET inhibition mitigates flares after inflammatory tissue priming *in vivo*.

To investigate the impact of I-BET151 on the first bout of arthritis and subsequent flare, we used a model that is based on two consecutive injections of inflammatory triggers, such as monosodium urate (MSU) crystals or zymosan, into the same paw of BALB/c mice (day 1 and day 9/10). After the first injection arthritis spontaneously resolves, while the second injection leads to a flare with delayed resolution of inflammation (6). Daily intraperitoneal (i.p.) injections of I-BET151, starting one day before initial induction of arthritis and continued until 9 days after flare induction (treatment group 1, Fig. 1A) did not significantly alter the first bout of MSU-induced arthritis, but reduced the flare (Fig. 1B, Fig. S1A). Histomorphometry on paws taken after the end of the experiment revealed that I-BET151-treated mice were characterized by reduced numbers of $TRAP^+$ osteoclasts and did not develop the massive bone erosions observed in twice injected primed (MSU/MSU) paws (Fig. 1C, 1D, S1B).

We have previously observed that inflammatory tissue priming is a stepwise, cumulative process worsening with repeated inflammatory insults (6). We thus asked if I-BET151 would work if given after resolution of the first bout of arthritis (paw thickness <120% of baseline normal paw thickness) and administered 6 daily i.p. injections before inducing the flare (days 4-9, treatment group 2, Fig. 1A). This treatment regimen was able to completely abrogate inflammatory tissue priming in MSU crystal-induced arthritis (Figs. 1E, S1C) and also significantly reduced it in zymosan-induced arthritis

Accepted Article

23265205, ja, Downloaded from https://onlinelibrary.wiley.com/doi/10.1002/art.42378 by Universität Bern, Wiley Online Library on [18/10/2022]. See the Terms and Conditions (https://onlinelibrary.wiley.com/terms-and-conditions) on Wiley Online Library for rules of use; OA articles are governed by the applicable Creative Commons License

(Figs. 1F, S1D). In contrast, a 3 day treatment preceding the second MSU crystal injection did not have a significant effect on tissue priming (treatment group 3, Figs. 1G, Fig S1E). The marked difference between 6 days and 3 days treatment prompted us to investigate if a longer pretreatment with I-BET151 would also influence acute inflammation during the first bout of arthritis. We therefore performed daily I-BET151 treatment for 6 days before the initial induction of arthritis (treatment group 1b, Fig. 1A). Similar to treatment group 1, the initial episode of arthritis was not affected, while the flare after repeated challenge was reduced (Figs. 1H, 1I, S1F). Thus, *in vivo* treatment with I-BET151 did not affect early inflammation during the first bout of arthritis, but diminished flares by interfering with inflammatory tissue priming.

In line with the importance of the acetylation state of histones in the development of inflammatory tissue priming, preventive *in vivo* treatment with the histone deacetylase inhibitor trichostatin A (TSA) (25, 26), that had been shown to induce senescence in SFs (27), also suppressed tissue priming (Fig. 1J). In contrast to BET inhibition, however, TSA also reduced the first arthritis episode (Figs. S1G, S1H). In contrast, treatment with the cytosine analog and DNA methyltransferase inhibitor decitabine, which had recently been shown to reduce T cell-dependent arthritis in mice (28) did not exhibit a significant effect on flares (Figs. 1J, S1G, S1H).

BET inhibition suppresses expansion of primed synovial fibroblasts and reverts changes in their gene expression and chromatin landscape

Previous studies have shown effects of BET inhibition on various cell types with potential importance for arthritis, among them macrophages, fibroblasts and osteoclast precursors (7). In line with a previous report (29) the number of mature $TRAP^+$ osteoclasts was significantly reduced during arthritis upon treatment with I-BET151 *in vivo* (Fig. S1B), and I-BET151 dose-dependently blocked the differentiation of murine osteoclast precursors into mature multinucleated osteoclasts *in vitro* (Fig. S2A, S2B).

To address the local cellular changes induced by I-BET151 treatment, we performed flow cytometry-based analysis of the composition of arthritis-relevant classical and non-classical immune cell types in the paw (Figs. 2A, S2C-S2E). Primed paws after two zymosan injections were characterized by significantly higher numbers of myeloid cells and neutrophils than -/zym contralateral paws that had been only injected once. Although there was a tendency towards reduced numbers of myeloid cells in zym/zym paws from I-BET151 treated mice, these changes were not statistically significant (Fig. S2D).

Enhanced HLA-DR expression on macrophages is a characteristic feature of arthritic joints (30) and is induced by IFNγ signaling, which happens to be a major mediator of inflammatory tissue priming (6). To assess macrophage activation in the joint, we measured MHC class II expression on $F4/80^+Ly6C^-$ synovial tissue macrophages (STMs). However, macrophage MHC II expression was not upregulated on STMs in primed (zym/zym) paws from vehicle-treated mice and even enhanced in STMs from zym/zym paws of I-BET151 treated mice (Fig. S2E). While the reasons for the upregulation of local macrophage MHC class II expression upon I-BET151 treatment are unclear, these data suggest that activation of STMs does not play a major role in inflammatory tissue priming and that the beneficial effects of I-BET151 treatment are likely mediated by other joint-residing cell populations.

We have shown before that tissue priming is driven by primed SFs characterized by specific changes in their gene expression and chromatin architecture (6). In line with that, flow cytometry demonstrated an expansion in primed paws of Podoplanin $(Pdpn)^+Thy1^+$ sublining fibroblasts, which

Accepted Article

23265205, ja, Downloaded from https://onlinelibrary.wiley.com/doi/10.1002/art.42378 by Universität Bern, Wiley Online Library on [18/10/2022]. See the Terms and Conditions (https://onlinelibrary.wiley.com/terms-and-conditions) on Wiley Online Library for rules of use; OA articles are governed by the applicable Creative Commons License

was significantly reduced in paws from I-BET151 treated mice. In contrast, the numbers of Thy1-negative SFs, which inhabit the synovial lining layer, were not affected by treatment with I-BET151 (Fig. 2A). By immunohistochemical analysis we also observed an enhanced abundance in primed (zym/zym) paws of fibroblasts expressing high amounts of Cadherin 11 (Cdh11), which mediates homotypic interactions between SFs and determines their pro-inflammatory behavior during arthritis (31). $Cdh11^+$ SFs were especially numerous in the pannus tissue in close proximity to degraded bone and less abundant in I-BET151 treated mice (Fig. 2B). Together, these data suggest that the expansion of pathogenic SFs during priming is reduced by I-BET151 treatment.

To shed light on the mechanisms underlying the effect of I-BET151 on fibroblasts, we performed bulk RNA-sequencing on cultured SFs from I-BET151-treated mice or upon I-BET151 treatment of primed (MSU/MSU) SFs *in vitro* (Figs. 2C-2F, S2F-S2H). Ingenuity pathway analysis identified 177 canonical pathways (Table S2) being differentially active in MSU/MSU SFs from mice treated with I-BET151 *in vivo* (treatment group 1) and 62 differentially regulated pathways in MSU/MSU SFs treated with I-BET151 *in vitro* (Table S3). Although the effect of *in vitro* treatment with I-BET151 was generally weaker than repeated administration *in vivo,* differentially regulated pathways largely overlapped between *in vivo* and *in vitro* treatment. Affected pathways were dominated by processes connected to inflammation, tissue remodeling, and cellular metabolism (Fig. 2D). Major inflammatory signaling pathways (e.g., TREM1, NF-κB, ILK and p38 MAPK signaling) were downregulated after I-BET151 treatment. I-BET151 additionally impacted several processes previously shown to be particularly connected with inflammatory tissue priming, for instance HIF-1α signaling, IL-6, inflammasomes and the complement system (6). Also major upstream regulators driving priming in SFs(6), e.g. IFNγ, IL-1β, and TNF, were downregulated by I-BET151 (Tables S2, S3). Gene set enrichment analysis (GSEA) (32) confirmed, among others, downregulation of the inflammatory response and the complement system upon I-BET151 treatment (Fig. S2G) and revealed that I-BET151 significantly downregulated a previously defined (6) set of genes specifically enriched in primed SFs (Fig. 2E). Enumeration of cell subpopulation frequencies from bulk RNA-Seq data by CIBERSORTx (22), using available scRNA-Seq profiles (6), demonstrated that treatment with I-BET151 particularly reduced the abundance of a cluster of sublining SFs, which express Thy1 and high amounts of complement C3 and are typically enriched in primed joints (Fig. 2F). Of note, the expression of members of the BET proteins (and also of the related family of bromodomain and plant homeodomain finger-containing proteins (33, 34), showed a trend to be downregulated in primed MSU/MSU as compared to -/MSU SFs, reaching the level of statistical significance for *Brd2*, *Brpf1* and *Brpf2* expression (Fig. S2H). This downregulation was significantly reverted by I-BET151 treatment for *Brd2* and *Brd4*. This is in line with upregulation of *Brd2* in bone marrow-derived macrophages and might indicate a compensation mechanism, where functional suppression of BET proteins leads to an increase in expression (13).

Synovial fibroblasts maintain their function and gene expression over many passages in culture, indicating the existence of stable epigenetic modifications. To integrate the expression changes in SFs after I-BET151 treatment with chromatin accessibility, we performed ATAC-Seq analysis on *in vitro*-treated SFs from primed (MSU/MSU) paws (Figs. 2G-2I, S2I). On a genome-wide level, I-BET151 treatment shifted chromatin accessibility of promotor regions in SFs from a primed (MSU/MSU) towards a -/MSU state (Fig. 2G). I-BET151 reduced chromatin accessibility at the transcription start sites (TSS) of many genes connected to inflammation (e.g., *Tnf*, *Il1a*, *Ccl3*, *Cxcl2*), inflammatory tissue priming (e.g., *C3*, *C3ar1*, *Il1b*, *Nlrp3*), matrix remodeling (e.g., *Mmp1b*, *Mmp9*), and metabolism (e.g. the glucose transporter *Slc2a6*) (Figs. 2H, 2I). There were also many genes that were downregulated on a transcriptional level after I-BET151 treatment but were not characterized by reduced

Accepted Article

23265205, ja, Downloaded from https://onlinelibrary.wiley.com/doi/10.1002/art.42378 by Universität Bern, Wiley Online Library on [18/10/2022]. See the Terms and Conditions (https://onlinelibrary.wiley.com/terms-and-conditions) on Wiley Online Library for rules of use; OA articles are governed by the applicable Creative Commons License

accessibility of their TSS, e.g., *Il6*, suggesting high specificity of control of gene expression by chromatin remodeling, as well as involvement of additional mechanisms of gene expression regulation (Fig. 2H). The entire lists of differentially regulated genes and differential accessible peaks in TSS are available in Tables S4 and S5, respectively. Thus, I-BET151 regulates gene expression and chromatin accessibility of genes connected to inflammatory tissue priming in a gene-specific manner.

BET inhibition aborts functional changes associated with primed synovial fibroblasts

The primed SF phenotype comprises arthritogenic function such as increased cytokine production, invasiveness, and an aberrant synovial lining formation.

To assess if *in vivo* treatment with I-BET151 affects SF function associated with priming, we isolated SFs from paws of I-BET151 and vehicle-treated mice (treatment group 1) and first assessed their capacity to build a synovial lining in 3D organ cultures as described (24). In line with previous findings (6), SFs from vehicle-treated primed (MSU/MSU) paws exhibited a decreased lining thickness as compared to -/MSU and naïve (-/-) cells. Instead, primed and also -/MSU SFs had a higher interconnectivity in the sublining of the organoid than naïve SFs. These characteristics of the synovial architecture of primed joints were normalized in SFs from I-BET151 treated mice (Figs. 3A, 3B). In fact, SFs from MSU/MSU paws of I-BET151 treated mice resembled the functional phenotype of naïve SFs. In line with these observations, the spontaneous release of inflammatory mediators, such as IL-1β, IFNβ and TNFα, from organoids formed by MSU/MSU SFs from I-BET151-treated mice was lower than from vehicle-treated mice, while the release of IL-8 and IL-6 was not significantly different (Fig. 3C).

Furthermore, SFs from I-BET151 treated mice exhibited reduced invasiveness in a matrix-associated transepithelial resistance invasion assay (Fig. 3D). Diminished invasiveness and migration were also observed in MSU/MSU SFs after treatment with Trichostatin A (Figs. S3A-3C).

BET inhibition resets the metabolic rewiring associated with fibroblast priming

During priming, SFs become metabolically invigorated, with a shift towards glycolysis (6). When analyzing the cellular metabolism by metabolic flux analysis of *in vitro* I-BET151 treated primed SFs we observed reduced glycolysis, while glycolytic reserve was enhanced (Figs. 3E, 3F, S3D, S3E). This observation is in line with reduced gene expression of key glycolytic enzymes such as alpha-enolase (*Eno1*), lactate dehydrogenase A (*Ldha*), aldolase C (*Aldoc*), 2,3-bisphosphoglycerate mutase (*Bpgm*), and pyruvate dehydrogenase kinase (*Pdk1*) after I-BET151 treatment, as assessed by RNA sequencing (Fig. S3F). In contrast to glycolysis, *in vitro* treatment with I-BET151 increased parameters of respiration (Figs. 3E, 3F, S3G, S3H). In consequence, the OCR/ECAR ratio was drastically higher in I-BET151-treated cells (Fig. 3E).

Glycolysis is a requirement for repeatedly triggered SFs to maintain viability and the primed functional phenotype (6). If metabolic rewiring does not take place, repeatedly stimulated fibroblasts fail to be primed and instead adopt a senescent immune-regulatory phenotype (35). In line with the inhibitory effect of I-BET151 on cellular metabolic reprogramming, SFs treated with I-BET151 *in vitro* demonstrated an increased accumulation of senescence-associated β-galactosidase when repeatedly challenged with TNFα *in vitro* (Fig. 3G). In aged I-BET151-treated MSU/MSU fibroblasts we also detected a significant upregulation of the senescence markers *p15* (*Cdkn2b*) and p21 (*Cdkn1a*) by real time quantitative PCR (Fig. 3H).

Flare reduction by BET inhibition *in vivo* is mediated by suppressive effects on fibroblast priming

To directly assess arthritogenicity of I-BET151 treated SFs, we used an established cell transfer model, where cultured primed SFs are injected into I paws to induce priming *in vivo* (6) (Fig. 4A).

Accepted Article

23265205, ja, Downloaded from https://onlinelibrary.wiley.com/doi/10.1002/art.42378 by Universität Bern, Wiley Online Library on [18/10/2022]. See the Terms and Conditions (https://onlinelibrary.wiley.com/terms-and-conditions) on Wiley Online Library for rules of use; OA articles are governed by the applicable Creative Commons License

Treatment of primed MSU/MSU SFs with I-BET151 *in vitro* before transfer reduced their ability to induce priming *in vivo* and to cause bone destruction and aberrant new bone formation along the metatarsals (Figs. 4B-E). Thus, I-BET151 interferes with the primed SF phenotype that mediates inflammatory tissue priming *in vivo*.

Clinical studies showed that systemic administration of BET inhibitors may lead to complication such as thrombocytopenia, neutropenia and male sterility (7, 36). Systemic administration of I-BET151 might therefore comprise considerable risks. We therefore investigated, if we could nullify inflammatory tissue priming by local administration of I-BET151 into the paw. 6 injections of I-BET151 into the MSU-injected paw antedating the second injection of MSU crystals (treatment group 2) significantly reduced inflammatory tissue priming (Figs. 4F, 4G), suggesting that local administration might be a practicable way to minimize systemic side effects of I-BET151 while maintaining its potential to inhibit flares.

I-BET151 induces functional and transcriptional changes in arthritis-derived and *in vitro*-primed human synovial fibroblasts

Changes in gene expression induced by I-BET151 treatment of human RA-derived SFs have been described (37), but effects of BET inhibition on pathways which are differentially regulated under repeatedly stimulated (primed) conditions have not been investigated yet. To translate our observations from mice to humans, we therefore primed human SFs derived from healthy joints by sequential incubation with TNFα as described (6, 16) and first performed transcriptional analysis by bulk RNA-Seq. Similarly to mouse-derived SFs, treatment with I-BET151 significantly impacted genes and canonical pathways related to fibroblast function, inflammation, and inflammatory tissue priming, such as e.g. wound healing, inflammatory cytokine networks, and interaction with classical immune cells such as granulocytes (Figs. 5A, 5B, S4A-S4C, Table S6). Similar to murine SFs, BET inhibition in human SFs also upregulated expression of most BET and BRDF proteins, with the increase in expression of *BRD2* and *BRPF2* reaching the level of statistical significance (Fig. S4C). Although not being among the top entries into the list of differentially regulated pathways, members of the complement system were also differentially regulated on RNA level and C3 activation was suppressed by I-BET151 on protein level (Figs. 5A, 5B, S4B, S4D, S4E).

Similarly to what we observed in murine SFs, I-BET151 also showed a trend to reduce the invasive capacity of *in vitro*-primed human SFs (Fig. 5D) and strongly increased senescence (Fig. 5E). Migration and invasion was also curbed in SFs from longstanding RA upon treatment with I-BET 151 *in vitro* (Figs. 5F, 5G).

Discussion

Herein we show that BET inhibition is not a general anti-inflammatory approach but selectively interferes with flares of inflammation in two mouse models of arthritis and inflammatory tissue priming. BET inhibition thereby reverses the local inflammatory priming of SF, associated with overshooting cytokine production and tissue destruction.

The synovial membrane is the primary site of pathology during the effector phase of arthritis and SFs act as key effector cells in joint inflammation and damage. Modern multi-omic profiling has revealed substantial functional heterogeneity of SFs in arthritis (38). During experimental arthritis and human RA, SFs become activated and form a pathological, highly organized sub-lining tissue, inhabited mostly by $Thy1^{+}CD34^{+}FAP\alpha^{+}$ SFs (4, 5). This special SF subset is also characterized by activation of the

Accepted Article

23265205, ja, Downloaded from https://onlinelibrary.wiley.com/doi/10.1002/art.42378 by Universität Bern, Wiley Online Library on [18/10/2022]. See the Terms and Conditions (https://onlinelibrary.wiley.com/terms-and-conditions) on Wiley Online Library for rules of use; OA articles are governed by the applicable Creative Commons License

intracellular complement system (the ´complosome´), metabolic invigoration and inflammasome activation and drives local susceptibility of and progressive worsening of arthritis (6).

Remodeling the epigenome is likely underlying these stable pathologic changes in SF gene expression and function (38, 39). For instance, DNA methylation patterns in SFs from RA patients are very distinct from those in osteoarthritis and SFs from non-inflamed individuals (40). Changes in DNA methylation are apparent already in very early stages of RA but are evolved further in longstanding RA (41, 42). The differentially methylated genes are critical to SF adhesion, trafficking, inflammation and extracellular matrix interactions (41-44).

With regards to histone modifications, higher marks of the active H3K4me3 and lower marks of the repressive H3K27me3 are present in the promoters of several matrix metalloproteinases (MMP) in RA-derived SFs (45). Increased histone acetylation is also apparent in the promoter of IL-6 (46). Acetylation of lysine reduces the positive charge on histones, thereby weakening their interaction with DNA and promoting a relaxed chromatin structure, which enables gene transcription. While histone acetylation and deacetylation are mediated by histone acetyltransferases (HATs) or histone deacetylases (HDACs), respectively, recognition of histone acetylation is a key event in the reading of epigenetic marks and is performed by BET proteins.

Dysregulation of BET proteins is particularly associated with the emergence of tumors (10) (e.g., mice overexpressing *Brd2* develop lymphomas (47), but single nucleotide polymorphisms in the *BRD2* locus were also found in RA patients (48). In consequence, inhibitors of BET proteins exhibit anti-cancer and anti-inflammatory activity (7, 9, 13). Several BET inhibitors have entered clinical trials for cancer, type 2 diabetes, cardiovascular disease and coronary artery disease.

We show here that the BET-protein inhibitor I-BET151 abrogated inflammatory tissue priming by reverting the primed phenotype of SFs and inhibits arthritis flares. SFs exposed to I-BET151 either *in vivo* or *in vitro* exhibited a reduced invasive capacity, migration and generally lowered capacity to prime tissue for inflammation and pathologic bone remodeling (49). I-BET151 treatment shifted gene expression towards resolution, supported by a metabolic shift from glycolysis towards OxPhos. Increased respiratory capacity in human SFs has recently been shown to be associated with resolution of synovitis (50). I-BET151 treatment also induced cellular senescence, heralded by increased expression of senescence-associated β-galactosidase.

The triazol ring of I-BET151 mimics the hydrogen bonding interactions essential for binding of the acetyl-lysine binding pocket to asparagine 140 and tyrosine 97 within the BRD. Importantly, BET inhibitors such as I-BET151 can also displace acetylated histone prebound to BRDs in macrophages and SFs (13, 51). Thus, they make a specifically interesting compound class for targeting established inflammatory tissue priming. In line, I-BET151 was even effective if administered after the first inflammatory insult and reverted the phenotype of already primed SFs.

In mice, I-BET151 conferred protection against LPS-induced endotoxic shock and bacteria-induced sepsis. I-BET 151 has also been shown efficient in K/BxN serum transfer arthritis (29) and BET inhibitors protect mice and rats from collagen-induced arthritis (7). The effects on CIA were mainly attributed to suppressive effects on Th17 cell differentiation and Th17-associated cytokines (52). However, how BET inhibitors target SF function and effect arthritis *in vivo* had not been addressed yet. Our results show that BET inhibition does not generally suppress arthritis, but interferes with the progressive worsening of flares caused by SF priming. Our results from mouse and human RA-derived and *in vitro*-primed SFs and previous studies in macrophages and human RA-SFs (13, 37) revealed that suppression of BET proteins has gene-specific effects, as BET proteins occupy super enhancers of transcription of genes that feature prominently under disease conditions, such as in tumorigenesis

Accepted Article

23265205, ja, Downloaded from https://onlinelibrary.wiley.com/doi/10.1002/art.42378 by Universität Bern, Wiley Online Library on [18/10/2022]. See the Terms and Conditions (https://onlinelibrary.wiley.com/terms-and-conditions) on Wiley Online Library for rules of use; OA articles are governed by the applicable Creative Commons License

and inflammation (53). BET inhibition was shown to primarily affect the expression of inflammation-associated secondary response genes from *de novo* enhancers that become activated at later points of macrophage activation. In contrast, promoters enriched for histone 3 and histone 4 acetylation and higher basal H3K4me levels, indicative of transcription during homeostasis, are less affected (13). In SFs, BET inhibitors decrease the TNFα, IL-1β and TLR ligand induced sustained inflammatory response and decrease SF proliferation and chemoattractance towards PBMCs (37. 39, 54). Silencing of BRD2 and BRD4 also downregulates MMP and cytokine expression in SFs, and BRD4 controls the migration and invasion of SFs (54).
In our study, I-BET151 effectively suppressed the expression of *Il6*, *Csf3*, *Il1a*, *Il1b*, and *Mmp1* in primed mouse and human SFs. I-BET151 also limited complement activation and tissue destruction by primed SFs, indicating the important role of BET proteins in inflammatory tissue priming. Furthermore, I-BET151 induced the expression of cyclin-dependent kinase inhibitors, implying that I-BET151 directs primed SFs towards senescence.

Our data show that *in vitro* treatment with I-BET151 before transfer significantly reduces the ability of primed SFs to sensitize the tissue for subsequent inflammation. Since in this experimental setup other arthritis-relevant cells have never been exposed to I-BET151, these results demonstrate that a significant part of I-BET151´s effect on priming and associated bone remodeling is mediated directly via SFs. However, in an *in vivo* situation SFs do of course not act in isolation, but in a dense interplay with other local and infiltrating cell types.
In our previous study we have observed that selective depletion of Cx3cr1-expressing synovial tissue macrophages reduced overall arthritis severity, but not tissue priming itself (6). Also in the current study, we have not found evidence that STMs influence the enhanced inflammation upon recurring arthritis or that I-BET151 would change the phenotype of STMs in a way that would impact inflammatory tissue priming. We can, however, not fully exclude that I-BET151´s action on other macrophage/monocyte subsets could contribute to arthritis severity or even tissue priming
Of note, I-BET151 treated mice had fewer $TRAP^+$ multinucleated osteoclasts in their inflamed paws and *in vitro* treatment with I-BET151 also dose-dependently suppressed osteoclast differentiation in nanomolar concentrations. It is not known which I-BET151 concentrations are reached in the paws, but especially upon local treatment it is likely that these effects contribute to some extent to the reduced bone destruction observed in I-BET151 treated mice.

In summary, BET inhibition appears as a promising therapeutic strategy to reset tissue priming and lower the susceptibility of tissue for inflammation.

Acknowledgements
We thank Uwe Appelt and Markus Mroz from the core unit for cell sorting and immunomonitoring at the Nikolaus-Fiebiger-Center for Molecular Medicine Erlangen for technical assistance with flow cytometry sorting of synovial fibroblasts. This work was supported by a fund from GlaxoSmithKline Research and development limited and the German Research Foundation (grant number FOR2886-TP08 to M.H.H. and D.M.).

Author contributions
Conceptualization: D.M., K.K., G.S., and M.H.H., Methodology: M.B., R.K., H.Z., Investigation: J.F., C.R., M.B., M.E., X.C., K.I.W., B.W., and D.W. Formal analysis: J.F., C.R., M.H., M.B., B.W., H.Z., D.W., P.K., K.K., and M.H.H., Resources: V.T. and V.T., Data Curation, A.B.E, P.K., H.Z., V.T.; Writing –

Accepted Article

23265205, ja, Downloaded from https://onlinelibrary.wiley.com/doi/10.1002/art.42378 by Universität Bern, Wiley Online Library on [18/10/2022]. See the Terms and Conditions (https://onlinelibrary.wiley.com/terms-and-conditions) on Wiley Online Library for rules of use; OA articles are governed by the applicable Creative Commons License

Original Draft, M.H.H.; Writing, Review & Editing, M.B., M.H., C.O., G.S. and M.H.H.; Visualization, M.B., D.W., K.K., M.H. and M.H.H.; Supervision and Project Administration, M.H.H.; Funding Acquisition, G.S., D.M. and M.H.H.

Conflict of interest statement

The authors declare no conflict of interest.

References

1. Kuijper TM, Lamers-Karnebeek FB, Jacobs JW, Hazes JM, Luime JJ. Flare Rate in Patients with Rheumatoid Arthritis in Low Disease Activity or Remission When Tapering or Stopping Synthetic or Biologic DMARD: A Systematic Review. J Rheumatol. 2015;42(11):2012-22.
2. Heckert SL, Bergstra SA, Matthijssen XME, Goekoop-Ruiterman YPM, Fodili F, Ten Wolde S, et al. Joint inflammation tends to recur in the same joints during the rheumatoid arthritis disease course. Ann Rheum Dis. 2021.
3. Alivernini S, MacDonald L, Elmesmari A, Finlay S, Tolusso B, Gigante MR, et al. Distinct synovial tissue macrophage subsets regulate inflammation and remission in rheumatoid arthritis. Nat Med. 2020;26(8):1295-306.
4. Croft AP, Campos J, Jansen K, Turner JD, Marshall J, Attar M, et al. Distinct fibroblast subsets drive inflammation and damage in arthritis. Nature. 2019;570(7760):246-51.
5. Zhang F, Wei K, Slowikowski K, Fonseka CY, Rao DA, Kelly S, et al. Defining inflammatory cell states in rheumatoid arthritis joint synovial tissues by integrating single-cell transcriptomics and mass cytometry. Nat Immunol. 2019;20(7):928-42.
6. Friscic J, Bottcher M, Reinwald C, Bruns H, Wirth B, Popp SJ, et al. The complement system drives local inflammatory tissue priming by metabolic reprogramming of synovial fibroblasts. Immunity. 2021.
7. Klein K. Bromodomain protein inhibition: a novel therapeutic strategy in rheumatic diseases. RMD Open. 2018;4(2):e000744.
8. Prinjha RK, Witherington J, Lee K. Place your BETs: the therapeutic potential of bromodomains. Trends Pharmacol Sci. 2012;33(3):146-53.
9. Filippakopoulos P, Picaud S, Mangos M, Keates T, Lambert JP, Barsyte-Lovejoy D, et al. Histone recognition and large-scale structural analysis of the human bromodomain family. Cell. 2012;149(1):214-31.
10. Fujisawa T, Filippakopoulos P. Functions of bromodomain-containing proteins and their roles in homeostasis and cancer. Nat Rev Mol Cell Biol. 2017;18(4):246-62.
11. Zou Z, Huang B, Wu X, Zhang H, Qi J, Bradner J, et al. Brd4 maintains constitutively active NF-kappaB in cancer cells by binding to acetylated RelA. Oncogene. 2014;33(18):2395-404.
12. Dey A, Chitsaz F, Abbasi A, Misteli T, Ozato K. The double bromodomain protein Brd4 binds to acetylated chromatin during interphase and mitosis. Proc Natl Acad Sci U S A. 2003;100(15):8758-63.
13. Nicodeme E, Jeffrey KL, Schaefer U, Beinke S, Dewell S, Chung CW, et al. Suppression of inflammation by a synthetic histone mimic. Nature. 2010;468(7327):1119-23.
14. Schauer C, Janko C, Munoz LE, Zhao Y, Kienhofer D, Frey B, et al. Aggregated neutrophil extracellular traps limit inflammation by degrading cytokines and chemokines. Nat Med. 2014;20(5):511-7.
15. Aletaha D, Neogi T, Silman AJ, Funovits J, Felson DT, Bingham CO, 3rd, et al. 2010 Rheumatoid arthritis classification criteria: an American College of Rheumatology/European League Against Rheumatism collaborative initiative. Arthritis Rheum. 2010;62(9):2569-81.
16. Crowley T, O'Neil JD, Adams H, Thomas AM, Filer A, Buckley CD, et al. Priming in response to pro-inflammatory cytokines is a feature of adult synovial but not dermal fibroblasts. Arthritis Res Ther. 2017;19(1):35.

Accepted Article

23265205, ja, Downloaded from https://onlinelibrary.wiley.com/doi/10.1002/art.42378 by Universität Bern, Wiley Online Library on [18/10/2022]. See the Terms and Conditions (https://onlinelibrary.wiley.com/terms-and-conditions) on Wiley Online Library for rules of use; OA articles are governed by the applicable Creative Commons License

Accepted Article

17. Ospelt C, Brentano F, Rengel Y, Stanczyk J, Kolling C, Tak PP, et al. Overexpression of toll-like receptors 3 and 4 in synovial tissue from patients with early rheumatoid arthritis: toll-like receptor expression in early and longstanding arthritis. Arthritis Rheum. 2008;58(12):3684-92.
18. Funakoshi-Tago M, Hattori T, Ueda F, Tago K, Ohe T, Mashino T, et al. A proline-type fullerene derivative inhibits adipogenesis by preventing PPARgamma activation. Biochem Biophys Rep. 2016;5:259-65.
19. Gonzalez-Navarro H, Abu Nabah YN, Vinue A, Andres-Manzano MJ, Collado M, Serrano M, et al. p19(ARF) deficiency reduces macrophage and vascular smooth muscle cell apoptosis and aggravates atherosclerosis. J Am Coll Cardiol. 2010;55(20):2258-68.
20. Russo D, Di Crescenzo RM, Broggi G, Merolla F, Martino F, Varricchio S, et al. Expression of P16INK4a in Uveal Melanoma: New Perspectives. Front Oncol. 2020;10:562074.
21. Love MI, Huber W, Anders S. Moderated estimation of fold change and dispersion for RNA-seq data with DESeq2. Genome Biol. 2014;15(12):550.
22. Newman AM, Steen CB, Liu CL, Gentles AJ, Chaudhuri AA, Scherer F, Khodadoust MS, Esfahani MS, Luca BA, Steiner D, et al. Determining cell type abundance and expression from bulk tissues with digital cytometry. Nat Biotechnol 2019; 37: 773-782.
23. Mizoguchi F, Slowikowski K, Wei K, Marshall JL, Rao DA, Chang SK, et al. Functionally distinct disease-associated fibroblast subsets in rheumatoid arthritis. Nat Commun. 2018;9(1):789.
24. Kiener HP, Watts GF, Cui Y, Wright J, Thornhill TS, Skold M, et al. Synovial fibroblasts self-direct multicellular lining architecture and synthetic function in three-dimensional organ culture. Arthritis Rheum. 2010;62(3):742-52.
25. Nasu Y, Nishida K, Miyazawa S, Komiyama T, Kadota Y, Abe N, et al. Trichostatin A, a histone deacetylase inhibitor, suppresses synovial inflammation and subsequent cartilage destruction in a collagen antibody-induced arthritis mouse model. Osteoarthritis Cartilage. 2008;16(6):723-32.
26. Jungel A, Baresova V, Ospelt C, Simmen BR, Michel BA, Gay RE, et al. Trichostatin A sensitises rheumatoid arthritis synovial fibroblasts for TRAIL-induced apoptosis. Ann Rheum Dis. 2006;65(7):910-2.
27. Nishida K, Komiyama T, Miyazawa S, Shen ZN, Furumatsu T, Doi H, et al. Histone deacetylase inhibitor suppression of autoantibody-mediated arthritis in mice via regulation of p16INK4a and p21(WAF1/Cip1) expression. Arthritis Rheum. 2004;50(10):3365-76.
28. Huang YS, Tseng WY, Clanchy FIL, Topping LM, Ogbechi J, McNamee K, et al. Pharmacological modulation of T cell immunity results in long-term remission of autoimmune arthritis. Proc Natl Acad Sci U S A. 2021;118(19).
29. Park-Min KH, Lim E, Lee MJ, Park SH, Giannopoulou E, Yarilina A, et al. Inhibition of osteoclastogenesis and inflammatory bone resorption by targeting BET proteins and epigenetic regulation. Nat Commun. 2014;5:5418.
30. Ridley MG, Panayi GS, Nicholas NS, Murphy J. Mechanisms of macrophage activation in rheumatoid arthritis: the role of gamma-interferon. Clin Exp Immunol. 1986; 63(3):587-93.
31. Lee DM, Kiener HP, Agarwal SK, Noss EH, Watts GF, Chisaka O, Takeichi M, Brenner MB. Cadherin-11 in synovial lining formation and pathology in arthritis. Science. 2007; 315(5814):1006-1010.32. Subramanian A, Tamayo P, Mootha VK, Mukherjee S, Ebert BL, Gillette MA, et al. Gene set enrichment analysis: a knowledge-based approach for interpreting genome-wide expression profiles. Proc Natl Acad Sci U S A. 2005;102(43):15545-50.
33. Klein K, Kato M, Frank-Bertoncelj M, Kolling C, Ciurea A, Gay S, Ospelt C. Evaluating the bromodomain protein BRD1 as a therapeutic target in rheumatoid arthritis. Sci Rep. 2018; 8(1):11125.
34. Igoe N, Bayle ED, Tallant C, Fedorov O, Meier JC, Savitsky P, Rogers C, Morias Y, Scholze S, Boyd H, Cunoosamy D, Andrews DM, Cheasty A, Brennan PE, Müller S, Knapp S, Fish PV. Design of a Chemical Probe for the Bromodomain and Plant Homeodomain Finger-Containing (BRPF) Family of Proteins. J Med Chem. 2017; 60(16):6998-7011.
35. Montero-Melendez T, Nagano A, Chelala C, Filer A, Buckley CD, Perretti M. Therapeutic senescence via GPCR activation in synovial fibroblasts facilitates resolution of arthritis. Nat Commun. 2020;11(1):745.

23265205, ja, Downloaded from https://onlinelibrary.wiley.com/doi/10.1002/art.42378 by Universität Bern, Wiley Online Library on [18/10/2022]. See the Terms and Conditions (https://onlinelibrary.wiley.com/terms-and-conditions) on Wiley Online Library for rules of use; OA articles are governed by the applicable Creative Commons License

Accepted Article

36. Shang E, Nickerson HD, Wen D, Wang X, Wolgemuth DJ. The first bromodomain of Brdt, a testis-specific member of the BET sub-family of double-bromodomain-containing proteins, is essential for male germ cell differentiation. Development. 2007;134(19):3507-15.
37. Klein K, Kabala PA, Grabiec AM, Gay RE, Kolling C, Lin LL, et al. The bromodomain protein inhibitor I-BET151 suppresses expression of inflammatory genes and matrix degrading enzymes in rheumatoid arthritis synovial fibroblasts. Ann Rheum Dis. 2016;75(2):422-9.
38. Marsh LJ, Kemble S, Reis Nisa P, Singh R, Croft AP. Fibroblast pathology in inflammatory joint disease. Immunol Rev. 2021;302(1):163-83.
39. Loh C, Park SH, Lee A, Yuan R, Ivashkiv LB, Kalliolias GD. TNF-induced inflammatory genes escape repression in fibroblast-like synoviocytes: transcriptomic and epigenomic analysis. Ann Rheum Dis. 2019;78(9):1205-14.
40. Ospelt C, Gay S, Klein K. Epigenetics in the pathogenesis of RA. Semin Immunopathol. 2017;39(4):409-19.
41. Ai R, Whitaker JW, Boyle DL, Tak PP, Gerlag DM, Wang W, et al. DNA Methylome Signature in Synoviocytes From Patients With Early Rheumatoid Arthritis Compared to Synoviocytes From Patients With Longstanding Rheumatoid Arthritis. Arthritis Rheumatol. 2015;67(7):1978-80.
42. Karouzakis E, Raza K, Kolling C, Buckley CD, Gay S, Filer A, et al. Analysis of early changes in DNA methylation in synovial fibroblasts of RA patients before diagnosis. Sci Rep. 2018;8(1):7370.
43. Nakano K, Whitaker JW, Boyle DL, Wang W, Firestein GS. DNA methylome signature in rheumatoid arthritis. Ann Rheum Dis. 2013;72(1):110-7.
44. Whitaker JW, Shoemaker R, Boyle DL, Hillman J, Anderson D, Wang W, et al. An imprinted rheumatoid arthritis methylome signature reflects pathogenic phenotype. Genome Med. 2013;5(4):40.
45. Araki Y, Tsuzuki Wada T, Aizaki Y, Sato K, Yokota K, Fujimoto K, et al. Histone Methylation and STAT-3 Differentially Regulate Interleukin-6-Induced Matrix Metalloproteinase Gene Activation in Rheumatoid Arthritis Synovial Fibroblasts. Arthritis Rheumatol. 2016;68(5):1111-23.
46. Wada TT, Araki Y, Sato K, Aizaki Y, Yokota K, Kim YT, et al. Aberrant histone acetylation contributes to elevated interleukin-6 production in rheumatoid arthritis synovial fibroblasts. Biochem Biophys Res Commun. 2014;444(4):682-6.
47. Greenwald RJ, Tumang JR, Sinha A, Currier N, Cardiff RD, Rothstein TL, et al. E mu-BRD2 transgenic mice develop B-cell lymphoma and leukemia. Blood. 2004;103(4):1475-84.
48. Mahdi H, Fisher BA, Kallberg H, Plant D, Malmstrom V, Ronnelid J, et al. Specific interaction between genotype, smoking and autoimmunity to citrullinated alpha-enolase in the etiology of rheumatoid arthritis. Nat Genet. 2009;41(12):1319-24.
49. Czegley C, Gillmann C, Schauer C, Seyler L, Reinwald C, Hahn M, et al. A model of chronic enthesitis and new bone formation characterized by multimodal imaging. Dis Model Mech. 2018;11(9).
50. Falconer J, Pucino V, Clayton SA, Marshall JL, Raizada S, Adams H, et al. Spontaneously Resolving Joint Inflammation Is Characterised by Metabolic Agility of Fibroblast-Like Synoviocytes. Front Immunol. 2021;12.
51. Krishna V, Yin X, Song Q, Walsh A, Pocalyko D, Bachman K, et al. Integration of the Transcriptome and Genome-Wide Landscape of BRD2 and BRD4 Binding Motifs Identifies Key Superenhancer Genes and Reveals the Mechanism of Bet Inhibitor Action in Rheumatoid Arthritis Synovial Fibroblasts. J Immunol. 2021;206(2):422-31.
52. Mele DA, Salmeron A, Ghosh S, Huang HR, Bryant BM, Lora JM. BET bromodomain inhibition suppresses TH17-mediated pathology. J Exp Med. 2013;210(11):2181-90.
53. Loven J, Hoke HA, Lin CY, Lau A, Orlando DA, Vakoc CR, et al. Selective inhibition of tumor oncogenes by disruption of super-enhancers. Cell. 2013;153(2):320-34.
54. Xiao Y, Liang L, Huang M, Qiu Q, Zeng S, Shi M, et al. Bromodomain and extra-terminal domain bromodomain inhibition prevents synovial inflammation via blocking IkappaB kinase-dependent NF-kappaB activation in rheumatoid fibroblast-like synoviocytes. Rheumatology (Oxford). 2016;55(1):173-84.

23265205, ja, Downloaded from https://onlinelibrary.wiley.com/doi/10.1002/art.42378 by Universität Bern, Wiley Online Library on [18/10/2022]. See the Terms and Conditions (https://onlinelibrary.wiley.com/terms-and-conditions) on Wiley Online Library for rules of use; OA articles are governed by the applicable Creative Commons License

Accepted Article

23265205, ja, Downloaded from https://onlinelibrary.wiley.com/doi/10.1002/art.42378 by Universität Bern, Wiley Online Library on [18/10/2022]. See the Terms and Conditions (https://onlinelibrary.wiley.com/terms-and-conditions) on Wiley Online Library for rules of use; OA articles are governed by the applicable Creative Commons License

Figure legends

Figure 1. Prevention and reset of inflammatory tissue priming by targeting histone acetylation. **(A)** Injection/treatment scheme for the inflammatory tissue priming models of arthritis. **(B)** Relative thicknesses of mouse paws injected once (-/MSU) or twice (MSU/MSU) with MSU crystals. Black arrowheads, MSU-injections; double arrow, length of treatment (treatment group 1). ANOVA with Tukey´s multiple comparisons test (AUC). N = 12-13 mice/group. **(C, D)** Representative tartrate-resistant acid phosphatase staining (C) and quantification of bone erosions (D) in the metatarsals of I-BET151/vehicle-treated mice (treatment group 1). N = 8 samples from individual mice/group. Red arrowheads indicate osteoclasts. Samples shown in (C) are indicated with a red dot in (D). Erosion index is the ratio between % eroded area in twice (MSU/MSU) and once (-/MSU) injected paws. Student´s t-test. **(E)** Time course and priming indices of iterated MSU-induced arthritis in vehicle-/I-BET151-treated mice (treatment group 2). Priming index is the ratio between AUC of the second episode of arthritis and the first episode of arthritis in the contralateral paw. Student´s t-test. N = 10 mice/group. **(F)** Priming indices of iterated zymosan-induced arthritis in vehicle/I-BET151-treated mice (treatment group 2). Student´s t-test. N = 7 mice/group. **(G)** Priming indices of iterated MSU-induced arthritis in treatment group 3. Student´s t-test. N = 13-14 mice/group. **(H)** Time course of iterated MSU-induced arthritis in vehicle-/I-BET151-treated mice (treatment group 1b). N = 10 mice/group. **(I)** Combined priming indices of treatment groups 1 and 1b. Student´s t-test. N =22-23 mice/group. **(J)** Priming indices of mice treated with trichostatin A (TSA), Decitabine, or vehicle. ANOVA with Dunnett´s Post hoc test. N = 6-7 mice per group.

Figure 2. Transcriptomic and chromatin analysis of synovial fibroblasts (SFs) after I-BET151 treatment. (A) Counts of total $CD45^{-}CD31^{-}Pdpn^{+}$ SFs, $Pdpn^{+}Thy1^{+}$ lining layer (LL) SFs and $Pdpn^{+}Thy1^{+}$ sublining (SL) SFs in paws from vehicle/I-BET151 treated mice (treatment group 2) 9 days after the 1^{st} /2^{nd} zymosan injection. ANOVA with Sidak´s multiple comparisons test. N = 4-5 samples of cells pooled from 2 mice each per group. **(B)** Immunohistochemical staining for Cadherin 11 (brown/black) in paws from vehicle/I-BET151 treated mice (treatment protocol 2) 9 days after the 1^{st}/2^{nd} zymosan injection. Scale bars, 200 µm **(C)** Volcano plots of differential gene expression in MSU/MSU SFs from I-BET151 vs vehicle-treated mice and in *in vitro* I-BET151 vs vehicle-treated MSU/MSU SFs. **(D)** Ingenuity pathway analysis showing selected canonical pathways differentially regulated in SFs after treatment with I-BET151 *in vivo* or *in vitro*. Dashed lines, adjusted p-value of 0.05. **(E)** Enrichment of a "Primed mouse-derived synovial fibroblasts" gene set (comprising the top-350 (by p-value) significant marker genes in primed murine SFs) in MSU/MSU SFs from vehicle-treated mice compared to either MSU/MSU SFs isolated from I-BET151 treated mice or upon I-BET151 treatment *in vitro.* NES, normalized enrichment score. **(F)** Relative frequencies of SL and LL fibroblasts in MSU/MSU paws from vehicle/I-BET151 treated mice, deconvoluted from bulk RNA Seq data using previously published scRNA-Seq profiles. Student´s t-test. N = 3 cell pools of 2 mice each per group. **(G)** Principal component analysis of -/MSU and primed (MSU/MSU) SFs treated *in vitro* with vehicle/I-BET151, based on the top 10,000 differentially accessible peaks from ATAC-Seq. **(H)** Log2 fold changes of expression of selected genes generated from RNA sequencing and ATAC Seq counts on annotated promoters, calculated as the ratio to the mean normalized counts from -/MSU SFs. Shown are pooled data from 3 replicates from cell pools of 2 mice each. **(I)** Representative genome tracks

displaying normalized profiles for RNA-Seq and ATAC-Seq signals around the *Nlrp3* gene. Each lane shows pooled data from 3 replicates of SF cultures from pools of 2 mice each.

Figure 3. I-BET151 treatment rectifies pathogenic function and metabolic changes of synovial fibroblasts (SFs) connected to inflammatory tissue priming. (A, B) Lining formation and interconnectivity (number of cell connections in the sublining) in 3D organ-cultures from SFs from paws of vehicle-/I-BET151-treated mice (treatment group 1). ANOVA with Sidak´s test. N = 3-7 SF-pools of 2 mice each per group. **(C)** Cytokines/chemokines in supernatants from 3D organ-cultures from primed SFs isolated from vehicle-/I-BET151-treated mice. Student´s t-test or Mann-Whitney U-test (IL-6). **(D)** Matrix invasion of SFs from I-BET151-/vehicle-treated mice (treatment group 1), assessed by decrease of transepithelial electrical resistance (TEER) indicating disturbance of an MDCK epithelial cell layer. Student´s t-test (n = 3-5 SF pools of 2 mice each per group). **(E, F)** Bioenergetics of MSU/MSU SFs (n = 5 SF pools of 2 mice each per group) treated with I-BET151/vehicle *in vitro*, as assessed by metabolic flux analysis normalized to background and total protein. Student´s t-test. **(G)** Percentages of senescence-associated beta galactosidase (SA-β-Gal)-positive TNF-primed SFs treated with I-BET151/vehicle *in vitro*. N = 3 SF pools from 2 mice each per group. Paired Student´s t-test. **(H)** Quantitative RT-PCR of *in vitro* vehicle/I-BET151-treated MSU/MSU SFs, showing expression of the senescence markers *Cdkn1a* (*p21*), *Cdkn2a* (*p16^{INK4}*), and *Cdkn2b* (*p15*). Paired Student´s t-test. N = 3 SF pools from 2 mice each per group.

Figure 4. Flare reduction by BET inhibition *in vivo* is mediated by suppressive effects on fibroblast priming (A-E) Arthritis and aberrant bone remodeling after injection of sorted cultured CD45$^-$CD31$^-$ naïve (-/-) or primed (MSU/MSU) SFs treated *in vitro* with I-BET151/vehicle into previously uninjected paws two days before MSU-injection. Shown are injection scheme **(A)**, course of arthritis **(B)** and priming indices **(C)**. Student´s t-test (n = 6 mice/group). **(D)** Representative 3D surface renderings and **(E)** quantification of osteophytes from microcomputed tomography scans of the metatarsals of MSU/MSU and -/MSU paws after injection of naïve or primed SFs treated *in vitro* with I-BET151/vehicle. Scale bars, 1 mm. N = 5-16 mice per group. Student´s t-test. Samples shown in (I) are indicated with a red dot. **(F)** Time course and priming indices of iterated MSU-induced arthritis upon daily local treatment with I-BET151/vehicle subcutaneously into the paw that had been previously triggered with MSU. Black arrowheads indicate MSU-injections into the paws, double arrow indicate length of treatment. Student´s t-test. N = 7 mice per group. **(G)** Representative 3D surface renderings from microcomputed tomography scans of the metatarsals of primed MSU/MSU paws after 6 subcutaneous injections of I-BET151/vehicle.

Figure 5. Functional and transcriptomic changes induced by BET inhibition in human synovial fibroblasts (SFs). (A) Ingenuity pathway analysis showing canonical pathways differentially regulated in SFs from healthy joints after repeated incubation with tumor necrosis factor (TNF) and treatment with I-BET151/vehicle in vitro. Dashed lines indicate an adjusted p-value of 0.05. **(B)** Expression of selected genes from bulk RNA-Seq of TNF-primed SFs from healthy joints upon treatment with I-BET151/vehicle (means from 3 replicates/group). **(C, D)** Matrix invasion of control and TNF-primed human SFs treated with I-BET151/vehicle. Shown are representative images (C) and quantification (D) of transmigrated crystal violet-stained SFs after 48h incubation with Platelet derived growth factor. N = 3 SF-cultures. Scale bars, 200 µm. Paired Student´s t-test. (E) Percentages of senescence-associated beta galactosidase (SA-β-Gal)-positive TNF-primed human SFs treated with I-BET151/vehicle. N = 4 SF cultures. Paired Student´s t-test. (F) Wound healing and migration of rheumatoid arthritis (RA)-derived SFs treated with I-BET151/vehicle. N = 4 SF cultures from individual

Accepted Article

23265205, ja, Downloaded from https://onlinelibrary.wiley.com/doi/10.1002/art.42378 by Universität Bern, Wiley Online Library on [18/10/2022]. See the Terms and Conditions (https://onlinelibrary.wiley.com/terms-and-conditions) on Wiley Online Library for rules of use; OA articles are governed by the applicable Creative Commons License

RA patients. Paired Student´s t-test. (G) Matrix invasion of vehicle-/I-BET151 treated RA-SFs, measured by the decrease of transepithelial electrical resistance (TEER) indicating disturbance of an MDCK epithelial cell layer. Paired Student´s t-test (n = 4 SF cultures from individual RA patients).

Accepted Article

23265205, ja, Downloaded from https://onlinelibrary.wiley.com/doi/10.1002/art.42378 by Universität Bern, Wiley Online Library on [18/10/2022]. See the Terms and Conditions (https://onlinelibrary.wiley.com/terms-and-conditions) on Wiley Online Library for rules of use; OA articles are governed by the applicable Creative Commons License

Accepted Article

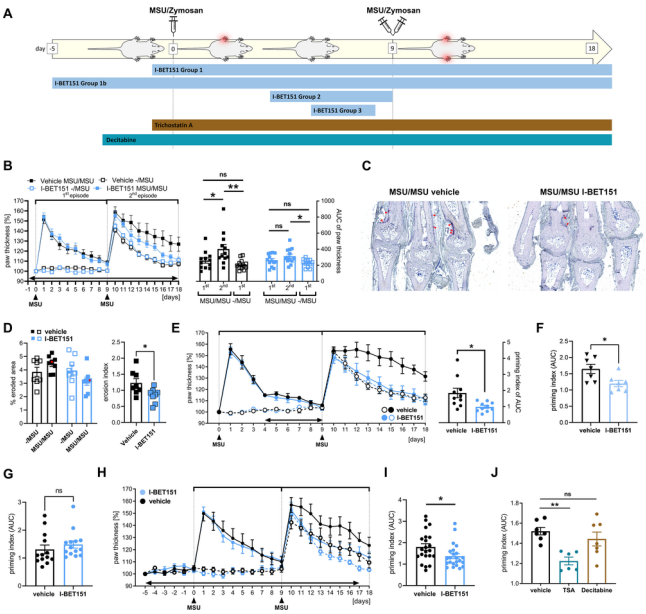

ART_42378_Fig1 revised.tif

23265205, ja, Downloaded from https://onlinelibrary.wiley.com/doi/10.1002/art.42378 by Universität Bern, Wiley Online Library on [18/10/2022]. See the Terms and Conditions (https://onlinelibrary.wiley.com/terms-and-conditions) on Wiley Online Library for rules of use; OA articles are governed by the applicable Creative Commons License

Accepted Article

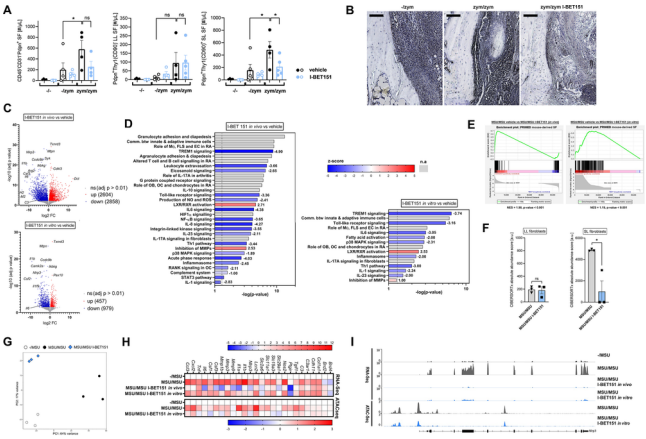

ART_42378_Fig2 revised.tif

23265205, ja, Downloaded from https://onlinelibrary.wiley.com/doi/10.1002/art.42378 by Universität Bern, Wiley Online Library on [18/10/2022]. See the Terms and Conditions (https://onlinelibrary.wiley.com/terms-and-conditions) on Wiley Online Library for rules of use; OA articles are governed by the applicable Creative Commons License

Accepted Article

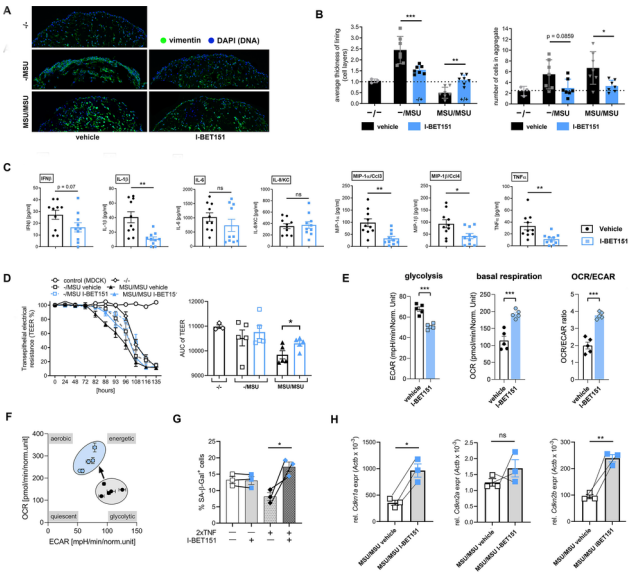

ART_42378_Fig3 final.tif

23265205, ja, Downloaded from https://onlinelibrary.wiley.com/doi/10.1002/art.42378 by Universität Bern, Wiley Online Library on [18/10/2022]. See the Terms and Conditions (https://onlinelibrary.wiley.com/terms-and-conditions) on Wiley Online Library for rules of use; OA articles are governed by the applicable Creative Commons License

Accepted Article

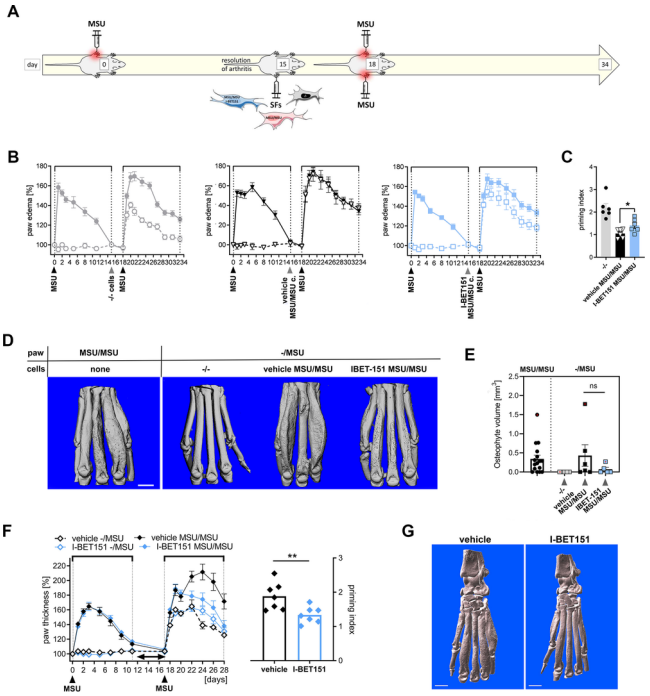

ART_42378_Fig4 final.tif

23265205, ja, Downloaded from https://onlinelibrary.wiley.com/doi/10.1002/art.42378 by Universität Bern, Wiley Online Library on [18/10/2022]. See the Terms and Conditions (https://onlinelibrary.wiley.com/terms-and-conditions) on Wiley Online Library for rules of use; OA articles are governed by the applicable Creative Commons License

Accepted Article

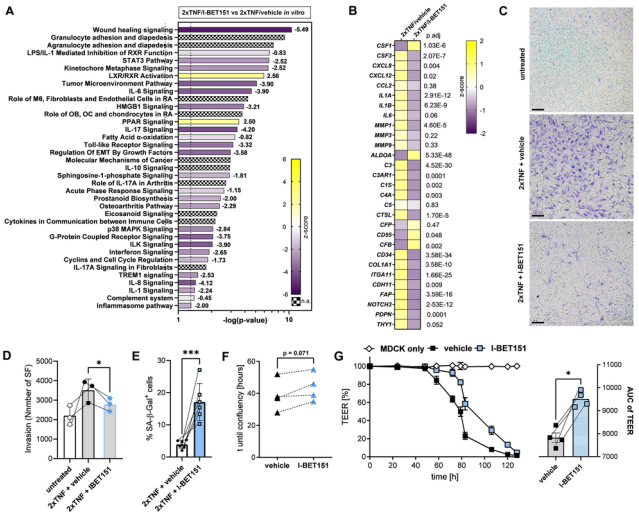

ART_42378_Fig5 final.tif

23265205, ja, Downloaded from https://onlinelibrary.wiley.com/doi/10.1002/art.42378 by Universität Bern, Wiley Online Library on [18/10/2022]. See the Terms and Conditions (https://onlinelibrary.wiley.com/terms-and-conditions) on Wiley Online Library for rules of use; OA articles are governed by the applicable Creative Commons License